Journal of Proteomics 207 (2019) 103467

Contents lists available at ScienceDirect

Journal of Proteomics

journal homepage: www.elsevier.com/locate/jprot

Quantitative proteomics reveals a Gα/MAPK signaling hub that controls pheromone-induced cellular polarization in yeast

Nicholaz Waszczak[a], Reagan DeFlorio[a], Amber Ismael[a], Naiyuan Cheng[a], David E. Stone[a,*], Metodi V. Metodiev[b,*]

[a] Department of Biological Sciences, University of Illinois at Chicago, 900 South Ashland Ave, Chicago, USA
[b] School of Life Sciences, University of Essex, Wivenhoe Park, Colchester, UK

ARTICLE INFO

Keywords:
Saccharomyces cerevisiae
Cell polarity
G proteins
Protein phosphorylation
MAPK kinase

ABSTRACT

The mating-specific yeast Gα controls pheromone signaling by sequestering Gβγ and by regulating the Fus3 MAP kinase. Disrupting Gα-Fus3 interaction leads to severe defects in chemotropism. Because Gα concentrates at the chemotropic growth site where Fus3 is required for the phosphorylation of two known targets, we screened for additional proteins whose phosphorylation depends on pheromone stimulation and Gα-Fus3 interaction. Using a mutant form of Gα severely defective in Fus3-binding, $G\alpha^{DSD}$, and quantitative mass spectrometry, fourteen proteins were identified as potential targets of Gα-recruited Fus3, ten of which were previously implicated in cell polarity and morphogenesis. To explore the biological relevance of these findings, we focused on the Spa2 polarisome protein, which was hypophosphorylated on multiple serine residues in pheromone-treated $G\alpha^{DSD}$ cells. Six sites were mutagenized to create the $Spa2^{6XSA}$ mutant protein. $Spa2^{6XSA}$ exhibited increased affinity for Fus3, consistent with a kinase-substrate interaction, and $Spa2^{6XSA}$ cells exhibited dramatic defects in gradient sensing and zygote formation. These results suggest that Gα promotes the phosphorylation of Spa2 by Fus3 at the cortex of pheromone-stimulated cells, and that this mechanism plays a role in chemotropism. How the Gα-Fus3 signaling hub affects the other putative targets identified here has yet to be determined.

Significance: Previously, interaction between the G alpha protein, Gpa1, and the MAPK of the pheromone response pathway, Fus3, was shown to be important for efficient sensing of the pheromone gradient and for the maintenance of cell polarity during mating. Here we show that the underlying molecular mechanisms involve the phosphorylation of specific cortical targets of Gpa1/Fus3. These have been identified by quantitative phosphoproteomics using a mutant of Gpa1, which is defective in interacting with Fus3. One of these targets is the polarisome protein Spa2. Alanine substitution of the Spa2 phosphorylation sites targeted by Gpa1/Fus3 lead to a dramatic defect in pheromone gradient sensing and zygote formation. These results reveal how the G alpha protein and the MAPK control cell polarity in a prototypical model system. Our results have wider significance as similar mechanisms exist in higher eukaryotes and are involved in important biological such as neuron development, immunity, and cancer cell metastasis.

1. Introduction

In the lifecycle of the unicellular eukaryote *Saccharomyces cerevisiae* (budding yeast), genetic recombination occurs when the organism switches between its haploid and diploid states. Haploid yeast exist as two mating types, *MAT***a** and *MAT*α, which can reproduce asexually by mitosis, or sexually, by fusing with cells of the opposite type. Cell and nuclear fusion (mating) produces *MAT***a**/*MAT*α diploids, which can then undergo meiosis to complete the sexual reproductive cycle. Because budding yeast cells are not motile, their ability to mate efficiently depends on chemotropism — the process by which cells sense the position of the nearest potential mating polarize their growth in that direction.

The yeast mating response is mediated by mating-type specific G-protein coupled receptors (GPCRs) and their cognate G protein. *MAT***a** and *MAT*α cells each secrete a peptide mating pheromone that binds to the receptor on cells of the other type. Pheromone-bound receptor activates the mating-specific Gα protein, Gpa1, which triggers phosphorylation of Gβ and dissociation of Gβγ from Gα-GTP. Free Gβγ then signals via a MAP kinase (MAPK) cascade to the nucleus, where the

* Corresponding authors.
E-mail addresses: dstone@uic.edu (D.E. Stone), mmetod@essex.ac.uk (M.V. Metodiev).

https://doi.org/10.1016/j.jprot.2019.103467
Received 3 June 2019; Received in revised form 20 July 2019; Accepted 23 July 2019
Available online 24 July 2019
1874-3919/

activated Fus3 MAPK induces cell-cycle arrest in G1 and mating-specific gene expression.

Once arrested in G1, pheromone-stimulated cells polarize their growth and form mating projections (also called shmoos) via actin-cable-directed delivery of membrane vesicles to a focused site (for reviews, see [1–3]. This process also locally concentrates the enzymes that degrade the cell wall and proteins that promote plasma membrane fusion during zygote formation [3]. In gradient-stimulated cells, Gβγ acts as a positional determinant by recruiting the Far1-Cdc24 adaptor-activator complex to the chemotropic growth site. In its role as an adaptor, Far1 binds directly to Gβγ and to the Bem1 scaffold protein; Cdc24 is the guanine nucleotide exchange factor that activates the conserved Rho-family GTPase, Cdc42 [4,5]. Activated Cdc42 (i.e., Cdc42-GTP) promotes the localization of Bem1 and the Bni1 formin protein to the incipient growth site via direct interaction. Because Bem1 interacts with Far1-Cdc24, additional Cdc42 is recruited to and activated at the growth site, thus initiating a positive feedback loop that results in the assembly of the polarisome — a protein complex consisting of Bni1, Spa2, Pea2 and Bud6. The polarisome nucleates actin filaments along which Myo2 carries secretory vesicles to the tip of the mating projection [6]. Thus, the receptor orients mating projection growth toward the source of pheromone by inducing local activation of Cdc42 and actin-cable nucleation via its G protein [7]. Pheromone-stimulated cells that are unable to sense a gradient (e.g., under isotropic or saturating-dose conditions), are also able to form mating projections: they shmoo where they would have budded in the next cell cycle [8]. This position, marked by Bud1, is known as the default polarity site [9].

Gα plays a critical role in chemotropism by directly interacting with activated Fus3 [10], and recruiting it to the cell cortex [11,12]. N-terminal myristoyl and palmitoyl moieties anchor Gα to the plasma membrane [13,14]. A mutant form of Gα that is defective in binding Fus3, $G\alpha^{DSD}$ (for Docking Site Disrupted), confers decreased mating efficiency and compromised partner discrimination, implying a handicap in pheromone-gradient sensing [10]. Although $G\alpha^{DSD}$ *BUD1* cells can form mating projections at the default polarity site, $G\alpha^{DSD}$ *bud1*Δ cells are unable to stably polarize their growth in response to pheromone, consistent with a role for the Gα-Fus3 interaction in establishing and/or maintaining the chemotropic growth site [15].

In mating cells, the pheromone receptor and its G protein polarize to the eventual chemotropic growth site prior to morphogenesis and remain concentrated in the growing region of the mating projection until the mating partners fuse. The direct interaction of Gα with activated Fus3 suggests that Gα recruits Fus3 to phosphorylate cortical targets at the chemotropic site. Gβ is likely to be one such target, as its pheromone-induced phosphorylation is substantially decreased in both *fus3*Δ and $G\alpha^{DSD}$ mutant strains [10,16]. Bni1 is likely to be another target of Gα-recruited Fus3. Matheos et al. showed that Fus3 phosphorylates Bni1, and that Fus3 is required for Bni1 localization to the shmoo tip [12]. Moreover, *fus3*Δ and $G\alpha^{DSD}$ were reported to phenocopy *bni1*Δ: pheromone-treated *bni1*Δ, *fus3*Δ, and $G\alpha^{DSD}$ mutants exhibit similar defects in microtubule alignment, and in the polarization of f-actin, Spa2-GFP, and GFP-Kar9. Together, these data suggest that Gα/Fus3-directed phosphorylation of Bni1 is essential to its mating-specific functions [12].

Recently, Errede et al. directly demonstrated that the Gα-Fus3 interaction is essential for chemotropism, as had been postulated based on genetic results [10], by assaying gradient tracking and morphogenesis in response to linear pheromone gradients generated in vitro [17]. Given that mating comprises a wide range of processes (e.g., gradient-oriented establishment of the growth site, polarized growth, cell wall and plasma membrane fusion, nuclear migration and fusion), that these processes all require the localization and regulated activation of numerous proteins at the chemotropic site, and that these proteins are frequently found to be phosphorylated on MAPK motifs in large-scale screens, we postulated that Gα directs Fus3 phosphorylation of mating-specific proteins in addition to Gβ and Bni1. To test this hypothesis, we used differential phosphoproteomic analysis to compare global protein phosphorylation in pheromone-treated Gα and $G\alpha^{DSD}$ cells. Our results indicate that the phosphorylation of ten known polarity proteins is significantly affected by $G\alpha^{DSD}$, suggesting that the Gα-Fus3 interaction is critical for spatial regulation of mating functions. This conclusion is supported by our study of the polarisome protein, Spa2, which appears to be targeted by Gα-Fus3 for phosphorylation on 6 serines. Alanine-substitution of these sites significantly increased the affinity of Spa2 for Fus3 but not for the Kss1 MAPK or cyclin-dependent kinases, and conferred clear defects in the ability of cells to orient and polarize toward their mating partners. These results provide additional evidence that Gα specifically recruits the pheromone-responsive Fus3 MAPK to phosphorylate Spa2, and that this is important for chemotropism.

2. Materials and methods

2.1. Microorganisms and culture conditions

Standard culturing and molecular techniques were used [18]. Yeast cells were cultured in either YEPD (1% yeast extract, 2% peptone, 2% dextrose) or in selective synthetic media (SS) (0.16% yeast nitrogen base, 0.5% ammonium sulfate, 2% dextrose, supplemented with the amino acids required for the SILAC experiments). L-arginine U-13C6, U-15N4 and L-lysine U-13C6, U-15N2 from Cambridge Isotope Laboratories were used at 100 mg/l in the SILAC experiments. Cells were grown at 30 °C and treated with alpha-factor pheromone (GeneScript) at 100 ng/ml for BF264-15D strains and at 4000 ng/ml for BY4741 strains. The lithium acetate method was used to transform yeast [19,20]; the electroporation method [21] was used to transform *E. coli* strain DH5α.

2.2. Plasmids and strains

The yeast strains used in this study (Supplementary Table 5) were derived from strain 15Dau (*MAT***a** *bar1Δ ade1 his2 leu2-3, -112 Δtrp1 ura3Δ*) [22], which is congenic with strain BF264-15D [23]. The $Spa2^{6XSA}$-GFP construct was created by overlap extension PCR mediated site directed mutagenesis using an XL II site directed mutagenesis kit (Agilent) and pRS406/Spa2p:Spa2-GFP (p406S2G; [24] as the template and the primers shown in Supplementary Table 6. The pRS406/Spa2p:Spa2-GFP and pRS406/Spa2p:$Spa2^{6XSA}$-GFP plasmids were linearized for integration into the genome of the *spa2*Δ derivative of strain BY4741 to generate strains NCY006 and NCY022, respectively, by cutting at a *BsaBI* recognition site, 76 base pairs upstream of the Spa2 start codon. A second *BsaBI* recognition site, 661 base pairs downstream of the *SPA2* start codon, appeared to have been blocked, likely by methylation. The in situ tagged *SPA2-GFP* and $spa2^{6XSA}$*-GFP* strains used for pull-down and mass spec analysis were created by deletion of native *SPA2* with *URA3* in the BY4741 *MAT***a** WT strain and subsequent transplacement of *URA3* with either *SPA2-GFP* or $spa2^{6XSA}$*-GFP*. *URA3p:URA3* was amplified from YCplac33 using *SPA2*-flanked *URA3* primers (#106 and #107, Supplementary Table 6). The linear PCR product was transformed into MSY101 to create the strain RDY321. *SPA2-GFP* and $spa2^{6XSA}$*-GFP* were amplified from pRS406/SPA2p:SPA2-GFP and pRS406/SPA2p:$spa2^{6XSA}$-GFP, *respectively,* using a forward *SPA2* primer and a *URA3*-flanked-*GFP* reverse primer (#111 and #108, respectively, Supplementary Table 6). The linear PCR products were transformed into RDY321 to create the strains RDY338 and RDY340, which were isolated by selection on synthetic media containing 2 mg/ml 5′FOA.

2.3. Preparation of yeast extracts for phospho-peptide analysis

SILAC was used to incorporate heavy-isotope containing amino acids into newly synthesized proteins in NWY023 and NWY025 cells.

SILAC heavy- and light-labeled cultures of both strains were allowed to proliferate or were treated with pheromone for 30 min. Cell pellets were lysed at 4 °C with 0.5 mm silica beads in 25 mM Tris-Cl buffer (150 mM NaCl, 10 mM Tris pH 8, 100 mM, 1% *v*/v Triton X100) containing phosphatase inhibitor (Roche) and protease inhibitor cocktails by manual vortexing with 30 s pulses. A minimum of 75% lysis was confirmed with phase contrast microscopy. Crude whole-cell lysates were centrifuged at 16,000 ×*g* at 4 °C for 20 min and protein concentrations were determined using a colorimetric protein assay kit (Bio-Rad). 3 mg total protein from the corresponding light and corresponding heavy-labeled lysates were mixed for both experimental protocols 1 and 2. Each crude lysate was normalized to 3 mg total protein and light vegetative lysates were mixed, in equal total protein amounts, with corresponding heavy labeled lysates of treated cells of the same strain. Lysate mixtures were diluted in 5× tris-glycine SDS sample buffer (0.25% bromophenol blue, 0.3 M DTT, 50% glycerol, 10% SDS, 0.25 M Tris-Cl pH 6.8) to 1× concentration, boiled for five minutes, and alkylated in the dark for 1 h with 60 mM iodoacetimide (Sigma-Aldrich). Samples were then centrifuged at 16,000 ×*g* for 15 min and loaded on a 10% self-cast 1 mm preparative tris-glycine poly-acrylamide gels, run 5 cm into the resolving layer and stopped. Gels were trimmed of excess material and stained using PageBlue protein staining solution (Fermentas) according to manufacturer's directions. Gels were manually sectioned into seven equal slices, cut manually into 1 mm × 1 mm cubes, and collected in low retention 1.7 ml centrifuge tubes (Kisker). Gel pieces were destained with consecutive incubations in three solutions; 50% methanol; 30 mM ammonium bicarbonate solution; and 50% acetonitrilile/30 mM ammonium bicarbonate solution. Destain cycles were repeated until gel pieces were visually void of dye, approximately three cycles. Gel pieces were dehydrated with 100% acetonitrile and vacuum centrifugation. Proteins were in-gel digested overnight at 30 °C with sequencing grade modified trypsin (Promega) diluted 1:40 in 30 mM ammonium bicarbonate solution. On the following day supernatant from in-gel digested samples was extracted by pipette and deposited into fresh low retention centrifuge tubes. Peptides were extracted with consecutive additions of Solution A (water with 0.1% formic acid, Fluka Analytical) and Solution B (acetonitrile with 0.1% formic acid, Fluka analytical) until gel pieces appeared visually dehydrated. Collected extracts were vacuum centrifuged to a pellet and enriched for phospho-peptides using a magnetic titanium dioxide phosphopeptide enrichment kit (Pierce) by following the manufacturer's directions. Lastly, pelleted phosphopeptides were resuspended in Solution A (Fluka Analytical) and analyzed by nano liquid chromatography electrospray ionization tandem mass spectrometry (nano LC-ESI-MS/MS) and MaxQuant [25] and Andromeda [26] as previously described [27,28].

2.4. Co-IP of Spa2-GFP and Spa2^{6XSA}-GFP in yeast

NWY091, NWY094, NWY095, MSY103, NCY003, NCY006, NCY016, NCY021 and NCY022 cells were cultured in duplicate to create parallel cultures for each strain. One set of cultures were treated with pheromone for 30 min and then dosed again. At 50 min post initial pheromone treatment, cultures were chilled on ice and harvested by centrifuging 3000 ×*g* for 2 min in a GS-3 rotor (Sorvall) at 4 °C. Cell pellets were washed with ice-cold water, frozen by dry-ice ethanol bath, and stored at −80 °C. Thawed cell pellets were resuspended in 750 µl GFP-Trap wash buffer (10 mM Tris/Cl pH 7.6, 150 mM NaCl, 0.5 mM EDTA) containing 1× protease inhibitor cocktail set III (Calbiochem). Cell suspensions were spilt across two 2 ml screw cap tubes (Midwest Scientific) and approximately 950 µl of ice-cold 0.5 mm zirconium/silica beads (BioSpec Products) were added. Mechanical lysis was performed by bead beating with a beadbeater-16 instrument (BioSpec Products) with fifteen 20 s pulses. Supernatants were separated from beads by pipetting with gel loading tips and split across two 2 ml centrifuge tubes, mixed with NP40 detergent (SigmaAldrich) to a final concentration of 0.5%, and incubated on ice for 10 min. Lysates were spun at 16,000 ×*g* for 10 min and supernatants were transferred to fresh centrifuge tubes and spun again. Supernatants were transferred to a second set of fresh centrifuge tubes and protein concentrations were determined with a 660 nm colorimetric based protein assay (ThermoFisher). 20ul magnetic GFP-TRAP slurry (Chromotek) was aliquoted into 2 ml centrifuge tubes and equalized in WASH buffer three times. 40 mg of each lysate was transferred into tubes containing equalized beads, refreshed with protease inhibitor cocktail and incubated with end-over-end rotation at 4 °C 2.5–3 h. After incubating, tubes were spun 4000 ×*g* for 3 min and supernatant was discarded. GFP-Trap beads were washed, five times, with WASH buffer. After the final wash, the WASH buffer was carefully removed with the aid of a gel loading pipette tip and bead slurries were resuspended in 25 µl 70 trypsin solution. The trypsin solution was prepared by diluting frozen trypsin (Promega) 40-fold in a solution of 30 mM ammonium bicarbonate with 1 M urea. Trypsin-treated bead mixtures were incubated overnight at 37 °C. Supernatants were extracted and desalted with 10 µl Zip Tips (Millipore) according to manufacturer's instructions with the following exceptions: 0.1% formic acid was substituted for TFA; a 200 µl tip was forced onto the Zip Tips to increase volume capacity; the wash volumes were 200 µl each. Desalted peptides were vacuum centrifuged until dry and analyzed with nano LC-ESI-MS/MS and Maxquant as previously described [27].

2.5. Zygote lysis analysis

Cultures of XWY054, NCY006, and NCY020 were grown to mid-log phase, and 2×10^7 cells were harvested by centrifugation. Cell pellets were resuspended in various volumes of water and briefly vortexed. Resupsension volumes were 1 ml for the 1× density, 500 µl for the 2× density, and 250 µl for the 4× density. Freshly diluted cultures were used to create mating mixtures in which XWY054 cells at a particular density were mixed with either NCY006 or NCY020 at the corresponding density, resulting in six separate mixtures. Mixed cultures were briefly vortexed and 10 µl of culture was deposited on a 1 cm diameter nitrocellulose filter, placed on a YEPD plate, and incubated at 30 °C for 2.5 h to allow for zygote formation. Filters were washed in 1 ml of water and 100 cells from each mating mixture were scored for normal and lysed zygotes with phase contrast microscopy. The data in Supplementary Table 4 represents the total number of cells for three independent trials at each density (n = 300).

For analysis using Trypan blue stain, cultures of XWY054, NCY006, and NCY020 were grown to mid-log phase, and 2×10^7 cells were harvested by centrifugation. Cell pellets were resuspended in 1 ml of media. Freshly diluted cultures were used to create mating mixtures in which XWY054 cells were mixed with either NCY006 or NCY020, resulting in two separate mixtures. Mixed cultures were briefly vortexed and then sonicated at 20% power for seven 0.5 s pulses. 10 µl of culture was deposited on a 1 cm diameter nitrocellulose filter, placed on a YEPD plate, and incubated at 30 °C for 2.5 h to allow for zygote formation. Filters were removed, placed in 1 ml of water, and vortexed for 1 min. Cells were pelleted and resuspended in 50 µl 0.2% Trypan Blue for 15′ at room temperature. 200 cells from each mating mixture were examined for Trypan blue staining. The data in Supplementary Table 4 represents the total number of cells for three independent trials (n = 600).

2.6. Fluorescence microscopy

Mating mixtures were prepared as described above for zygote lysis analysis with the exception that the mixtures were deposited on agarose

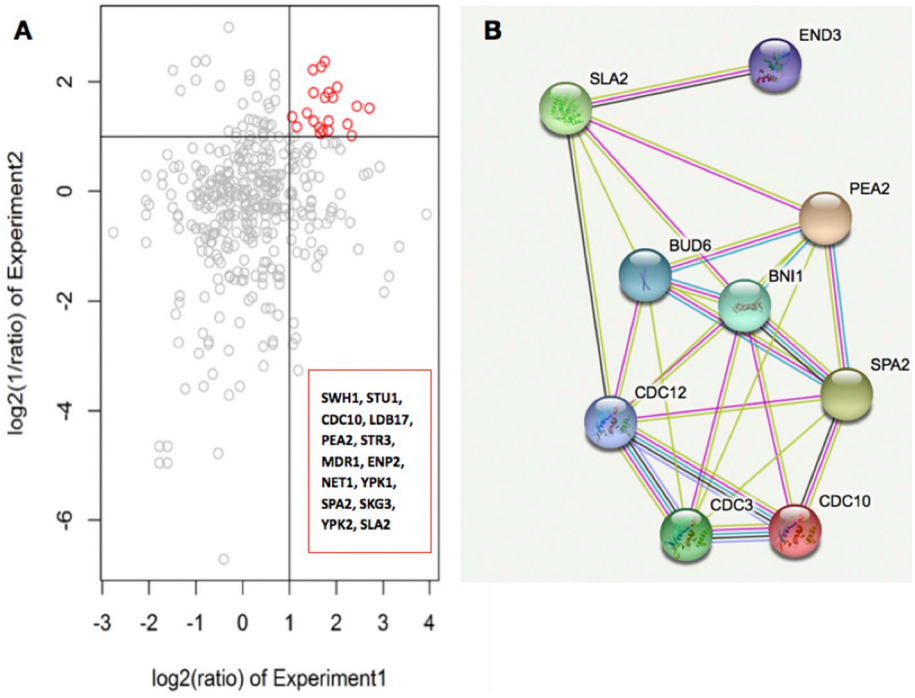

Fig. 1. Quantitative analysis of yeast phosphoproteome during mating in Gα and Gα^{DSD} cells. **A**. Cells were labeled as described in Materials and Methods and treated with pheromone for 30 min. The phosphopeptides were isolated by TiO_2-affinity chromatography and quantified by LC-MS/MS. The x-axis coordinates show the log2 transformed ratio obtained by dividing the normalized H/L ratios from Gα^{WT} cells by the normalized H/L ratios obtained from Gα^{DSD} cells for the same phosphopeptide in experiment 1, in which the heavy-labeled cells were treated with pheromone and Gα^{DSD} and Gα^{WT} were analyzed separately. The y-axis coordinates show the log2-transformed normalized L/H SILAC ratios from experiment 2, in which pheromone-treated Gα^{DSD} and Gα^{WT} cells were analyzed as a single sample. The Gα^{DSD} cells were heavy-labeled. **B**. STRING database analysis of the identified proteins. For description of STRING see [42]. The three polarity proteins, Spa2, Pea2, and Sla2, and CDC10, are part of tightly connected module. The STRING protein-protein interaction enrichment (PPI) *p*-value for this network is 3.38e-08.

pads composed of selective synthetic media. Mating mixtures were imaged every 5 min for 3 h using a DeltaVision Elite deconvolution microscope (Applied Precision). Images were captured by 60× objective with 488 nm laser excitation set to 10% with 150 ms exposure, 10-slice 0.5 μm z-stacks were taken at each time point. Fiji image processing software was used to merge fluorescent and DIC captured images and encoded to 8-bit stacked TIFF files. Individual images were pulled from stacked TIFF files by use of Fiji.

2.7. Statistical analysis

R. Student's *t*-test, Fisher exact test, and Chi-squared tests were computed using the *t*-test, fisher exact test and chi-squared test functions. *P* value adjustment for multiple testing was done using the false discovery rate method. Gene ontology term enrichment was calculated using the YeastMine database described in Balakrishnan et al. [30].

3. Results

3.1. Gα^{DSD} compromises the pheromone-induced phosphorylation of multiple proteins involved in cell polarization

To identify putative substrates of Gα-recruited Fus3, we used the stable isotope labeling by amino acids in culture (SILAC) approach for quantitative phosphoproteomics [29]. We looked for proteins that were more efficiently phosphorylated in pheromone-treated cells expressing Gα than in cells expressing Gα^{DSD}. Growing cells both in normal medium and in medium containing amino acids labeled by heavy-isotopes enabled us to simultaneously analyze the phospho-peptides in the lysates from two cultures at once, thereby minimizing differences due to instrument and sample-handling variance, and increasing the precision of peptide quantitation. We took advantage of this capability to make two comparisons. By using two different labeling protocols, we also minimized the chance of misleading results due to isotope-related effects on protein abundance or phosphorylation. In the first experiment, we determined the effect of pheromone treatment on the phosphoproteome of a given strain (i.e, strain held constant; condition varied), analyzing cells expressing wild type Gα and Gα^{DSD} in this way. Vegetative cells were grown in normal light medium (henceforth, L), while cells to be pheromone-treated were first labeled with heavy amino acids (henceforth, H). The two cultures were then mixed and analyzed as a single sample. An H/L ratio > 1 for a given phosphopeptide therefore indicates that its phosphorylation is induced by pheromone. The resulting data sets allowed us to ask whether Gα^{DSD} affects pheromone-induced phosphorylation by dividing the H/L ratio of a given phosphopeptide in the control (WT Gα) cells by its H/L ratio in the experimental (Gα^{DSD}) cells. Values > 1 indicate that Gα^{DSD} confers hypophosphorylation. In the second experiment, pheromone-treated control cells were grown in normal medium and pheromone-treated Gα^{DSD} cells were pre-labeled in heavy medium (i.e., condition held constant; strain varied); the two cultures were then mixed and analyzed as a single sample. In this protocol H/L ratio < 1 for a given phosphopeptide suggests decreased phosphorylation in Gα^{DSD} cells.

We identified candidate Gα-Fus3 target proteins by looking for H/L ratios relating the relative degree of pheromone-induced phosphorylation in Gα and Gα^{DSD} cells beyond stringent threshold values (> 2 for the experiment 1 calculation and < 0.5 for the experiment 2 calculation). Fourteen proteins met these criteria: Cdc10, Enp2, Ldb17, Mdr1, Net1, Pea2, Skg3, Sla2, Spa2, Str3, Stu1, Swh1, Ypk1, and Ypk2 (Fig. 1 and Table 1). Several proteins were identified with more than one phosphopeptide and several peptides were phosphorylated on more than one residue. In total, we found 21 sites that were hypophosphorylated in pheromone-treated Gα^{DSD} cells in both experiments 1 and 2, of which seven were canonical MAPK sites: S or T followed by P. These were as follows: one SP site in Swh1; two SP sites in Pea2; one TP site in Ypk1; one SP site in Spa2; one TP and one SP site in Sla2.

Candidate proteins were analyzed for gene ontology (GO) term enrichment using the *Saccharomyces* Genome Database (SGD) data retrieval tool, YeastMine [30]. Groups of the candidate genes enriched for specific GO terms (adjusted $p < .05$) in the "biological process" ontology are shown in Table 1. The GO terms associated with our identified genes group with highest statistical significance were *cytokinesis*

(*CDC10*, *NET1*, *PEA2*, *SLA2* and *SPA2*; $p < .002$); *bud site-selection* (*PEA2*, *SPA2*, and *SLA2*; $p < .006$); *establishment and maintenance of cell polarity* (*SWH1*, *CDC10*, *PEA2*, *SPA2*, and *SLA2*; $p < .006$); *regulation of cell morphogenesis* (*PEA2*, *SPA2*, *YPK2*; $p < .02$), and *regulation of mating projection growth* (*SPA2* and *PEA2*; $p < .02$). Groups of the candidate genes enriched for specific GO terms ($p < .05$) in the "cellular component" ontology are shown in Table 2. The GO terms associated with our identified genes group with highest statistical significance were *cellular bud* and *site of polarized growth* (*CDC10*, *LDB17*, *PEA2*, *YPK1*, *SPA2*, *SKG3*, and *SLA2*; $p < .0003$), and *cell projection*, *mating projection tip*, *cell projection part*, and *mating projection* (*CDC10*, *PEA2*, *SPA2* and *SLA2*; $p < .02$).

Although $G\alpha^{DSD}$ dramatically decreased pheromone-induced phosphorylation of numerous cortical proteins, it had no such effect on the phosphorylation of the mating-specific transcriptional inhibitor, Dig2, a well-known nuclear target of Fus3 (Supplementary Table 1). Pheromone-induced phosphorylation of Dig2 residue S225 was detected in both experiments 1 and 2, consistent with published reports [31], and did not significantly differ in $G\alpha^{DSD}$ and $G\alpha^{WT}$ cells. In experiment 1, the H/L ratios of the S(ph)PHIEDITSR Dig2 peptide were 1.78 and 2.45 in $G\alpha^{DSD}$ and $G\alpha^{WT}$ cells, respectively; In experiment 2, the DSD/WT ratio was 0.94. These results demonstrate very similar levels of the Dig2 phosphorylated peptide in the pheromone-treated $G\alpha^{DSD}$ and $G\alpha^{WT}$ cultures.

It is notable that our phosphoproteomic screen did not detect phospho-peptides derived from Bni1 and Ste4 — proteins thought to be substrates of Gα -Fus3 [10,12,16]. The most likely reason for not detecting these proteins is the scale of the phosphoproteomics experiment, which did not allow exhaustive and comprehensive interrogation of the yeast phosphoproteome. As described in the Materials and Methods, we used a relatively small amount of starting material, 3 mg total protein, and gel-based separation of the labeled intact proteins. Denaturing electrophoresis as a front-end separation increases resolution but limits capacity. Phospho-peptides derived from low-abundance proteins may therefore fall below the threshold for detection. In addition, phospho-peptides with low phosphorylation stoichiometry are less likely to be detected at this scale of analysis.

3.2. The $gpa1^{DSD}$ mutation confers a dramatic decrease in the abundance of a large number of proteins in pheromone-treated cells

In addition to identifying putative targets of pheromone-induced Gα/Fus3 phosphorylation by phosphoproteomic analysis, we evaluated the effect of breaking the Gα-Fus3 interaction on protein levels by analyzing the total proteome of Gα and $G\alpha^{DSD}$ cells. The results suggest that in pheromone-treated cells, $G\alpha^{DSD}$ causes a significant decrease in the abundance of a large set of proteins, and that this set is highly enriched for proteins involved in the regulation of vesicle trafficking and protein localization (Supplementary Table 2). Using the criterion that a protein must show at least a 2-fold decrease in $G\alpha^{DSD}$ cells and no change or an increase in Gα cells, we identified 418 proteins with decreased abundance in pheromone-treated $G\alpha^{DSD}$ cells. We used GO term enrichment analysis to compare this group to 1054 proteins that were either unchanged or increased in abundance in both Gα and $G\alpha^{DSD}$ cells. This analysis showed that:

1. Among the 418 proteins whose abundance was significantly decreased in $G\alpha^{DSD}$ cells, 13.2% are assigned to the *Golgi vesicle*

Table 1
Enriched GO terms in the ontology "Biological process".

Biological process term	Adjusted *p*	Standard gene name
Cytoskeleton-dependent cytokinesis	0.001512	*CDC10, PEA2, NET1, SPA2, SLA2*
Mitotic cytokinesis	0.001906	*CDC10, PEA2, NET1, SPA2, SLA2*
Cytokinesis	0.001925	*CDC10, PEA2, NET1, SPA2, SLA2*
Bipolar cellular bud site selection	0.005336	*PEA2, SPA2, SLA2*
Establishment or maintenance of cell polarity	0.005714	*SWH1, CDC10, PEA2, SPA2, SLA2*
Mitotic cytokinetic process	0.007429	*PEA2, NET1, SPA2, SLA2*
Cytokinetic process	0.014383	*PEA2, NET1, SPA2, SLA2*
Regulation of cell morphogenesis	0.01711	*PEA2, SPA2, YPK2*
Regulation of initiation of mating projection growth	0.01857	*PEA2, SPA2*
Regulation of termination of mating projection growth	0.01857	*PEA2, SPA2*
Regulation of anatomical structure morphogenesis	0.025303	*PEA2, SPA2, YPK2*
Mitotic cell cycle	0.028985	*STU1, CDC10, PEA2, NET1, SPA2, SLA2*
Endocytosis	0.029205	*SWH1, LDB17, YPK1, SLA2*
Cytoskeleton organization	0.029684	*STU1, CDC10, PEA2, SPA2, SLA2*
Regulation of mating projection assembly	0.030869	*PEA2, SPA2*
Regulation of developmental process	0.03111	*PEA2, SPA2, YPK2*
Cellular bud site selection	0.031584	*PEA2, SPA2, SLA2*
Mitotic cytokinesis, site selection	0.031584	*PEA2, SPA2, SLA2*
Cell division	0.032012	*STU1, CDC10, PEA2, NET1, SPA2, SLA2*
Mitotic cell cycle process	0.03256	*STU1, CDC10, PEA2, NET1, SPA2, SLA2*
Cell morphogenesis	0.036133	*PEA2, SPA2, YPK2*
Regulation of cell projection organization	0.036298	*PEA2, SPA2*
Regulation of cell projection assembly	0.036298	*PEA2, SPA2*
Eisosome assembly	0.036298	*YPK1, YPK2*
Mating projection assembly	0.036995	*PEA2, SPA2*
Regulation of actin cytoskeleton reorganization	0.036995	*PEA2, SPA2*
Positive regulation of actin cytoskeleton reorganization	0.036995	*PEA2, SPA2*
Cytokinesis, site selection	0.03794	*PEA2, SPA2, SLA2*
Regulation of cellular component biogenesis	0.03819	*PEA2, NET1, YPK1, SPA2*
Membrane invagination	0.041157	*SWH1, LDB17, YPK1, SLA2*
Cell budding	0.042119	*PEA2, SPA2, SLA2*
Asexual reproduction	0.042119	*PEA2, SPA2, SLA2*
Cell projection organization	0.04353	*PEA2, SPA2*
Cell projection assembly	0.04353	*PEA2, SPA2*

Table 2
Enriched GO terms in the ontology "Cellular component".

Cellular component term	Adjusted *p*	Standard gene name
Cellular bud	0.000169	*CDC10, LDB17, PEA2, YPK1, SPA2, SKG3, SLA2*
Site of polarized growth	0.000239	*CDC10, LDB17, PEA2, YPK1, SPA2, SKG3, SLA2*
Cellular bud neck	0.000295	*CDC10, LDB17, PEA2, YPK1, SPA2, SKG3*
Cellular bud tip	0.013322	*PEA2, SPA2, SKG3, SLA2*
Polarisome	0.014016	*PEA2, SPA2*
Cell projection	0.016387	*CDC10, PEA2, SPA2, SLA2*
Mating projection tip	0.017665	*CDC10, PEA2, SPA2, SLA2*
Cell projection part	0.018949	*CDC10, PEA2, SPA2, SLA2*
Mating projection	0.019307	*CDC10, PEA2, SPA2, SLA2*
Cell cortex part	0.019307	*CDC10, LDB17, PEA2, SPA2, SLA2*
Incipient cellular bud site	0.027427	*PEA2, SPA2, SLA2*
Cell cortex	0.030051	*CDC10, LDB17, PEA2, SPA2, SLA2*
Cytoplasmic region	0.030051	*CDC10, LDB17, PEA2, SPA2, SLA2*

transport category (GO:0048193) and 57.4% to the *cellular component organization or biogenesis* category (GO:0071840), as compared to 1.6% (p = 5.492231e-18) and 32.9% (p = 1.019308e-17), respectively, of the 1054 proteins whose abundance was unaffected by $G\alpha^{DSD}$.

2. Among the genes that are upregulated or unchanged in both strains, *small molecule metabolic process* (GO:0044281) is the top enriched category in upregulated or unchanged group of genes (SILAC ratio DSD $\geq$0.80, WT $\geq$0.8).

Five out of the 14 proteins shown in Fig. 1 were also found in the group of proteins whose abundance was significantly decreased in pheromone-treated $G\alpha^{DSD}$ cells. These are Cdc10, Net1, Ypk2, Spa2, and Sla2. SILAC quantification data showing the effect of $G\alpha^{DSD}$ on three representative proteins is shown in Fig. 2.

Taken together, the phosphoproteomic analysis and the total proteome quantitation data suggest that Gα-directed Fus3 phosphorylation of cortical substrates that play a role in cell polarity has a stabilizing effect on a large number of proteins involved in trafficking and localization.

3.3. *SPA2 mutagenesis and pull-down experiments confirm Spa2 as a target of Fus3 during the pheromone response*

Our differential phosphoproteome analysis revealed that pheromone-treated $G\alpha^{DSD}$ cells hypophosphorylate six Spa2 residues (S254, S274, S585, S646, S979, and S1263 (Supplementary Table 1). Among the proteins shown in Fig. 1, Spa2 had the highest number of differentially phosphorylated sites, but hypophosphorylation of only one Spa2 peptide correlated with $G\alpha^{DSD}$ in both experiments; five additional hypophosphorylated Spa2 sites were detected in either one experiment or the other. These six sites were also identified in a large-scale analysis of phospho-peptide isolated from pheromone-treated cells [32]. Spa2 is a constituent of the polarisome, along with Bni1, Pea2 and Bud6. A priori, phosphorylation of Spa2 could affect its affinity for other members of the polarisome and/or its ability to localize to the site of polarized growth. As a first step toward understanding the role of Gα/Fus3-dependent phosphorylation of Spa2, we constructed $Spa2^{6XSA}$-GFP, a GFP-tagged mutant form of Spa2 in which all six of the serine residues identified in our analysis were changed to alanine. We then created *spa2*Δ strains transformed with integrative vectors carrying either $Spa2^{6XSA}$-GFP or Spa2-GFP, and strains in which we used the $Spa2^{6XSA}$-GFP and Spa2-GFP constructs to replace the native copy of *SPA2*.

To determine whether mutation of the six putative Gα/Fus3-dependent Spa2 phosphorylation sites affects the affinity of Spa2 for its

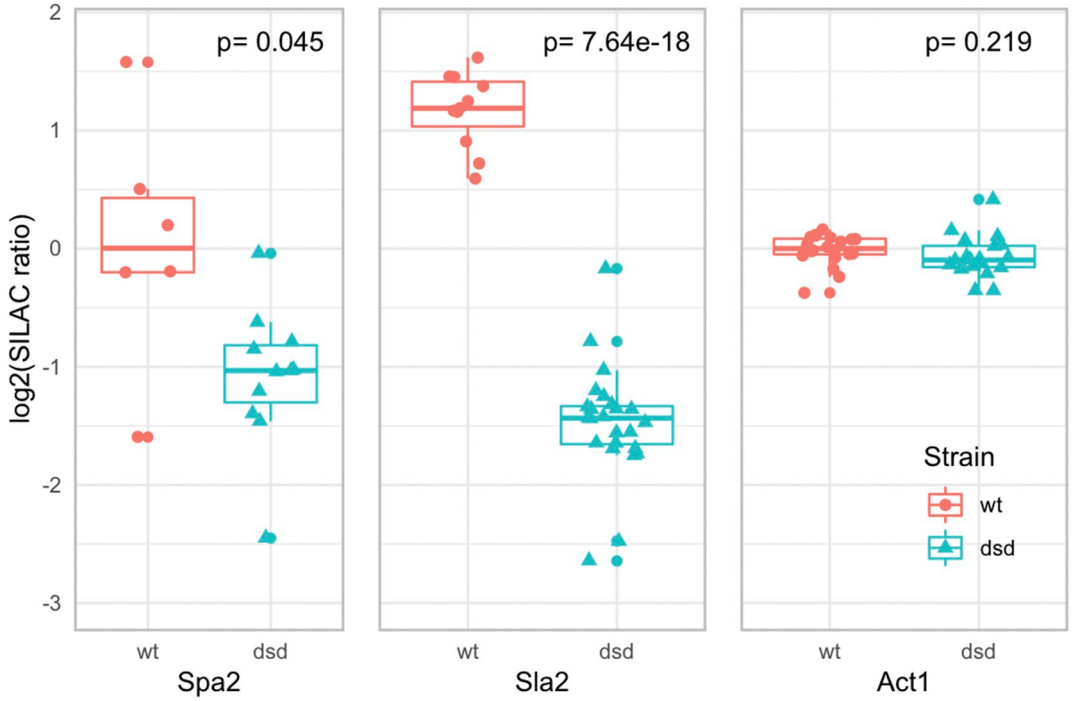

Fig. 2. Effect of pheromone treatment on Spa2, Sla2, and Act1 abundance in Gα and $G\alpha^{DSD}$ cells. The boxplots show log2-transformed normalized H/L ratios for the individual peptides as reported by MaxQuant. The heavy SILAC-labeled cells were treated with pheromone. The *p*-values were computed using the Student's *t*-test in R. The data is from a single labeling experiment.

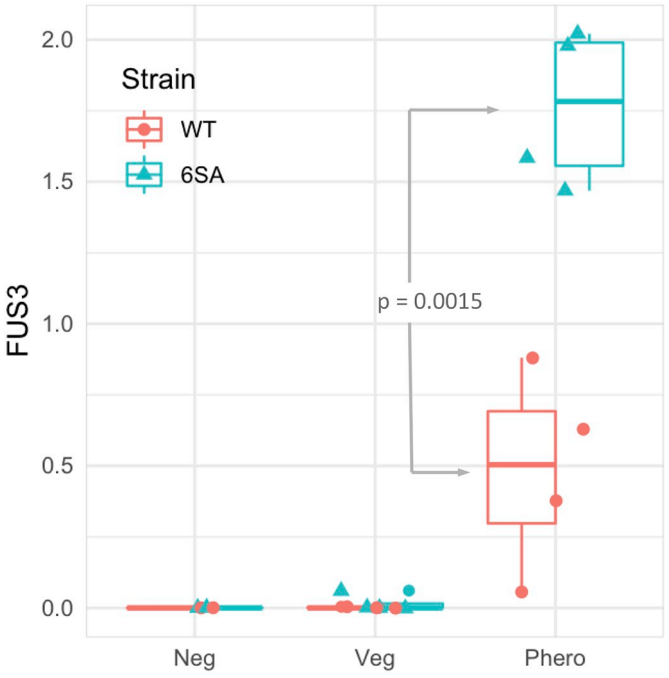

Fig. 3. Boxplots showing normalized and scaled Fus3 intensity in Spa2-GFP and Spa2^{6xSA}-GFP immunoprecipitates obtained from vegetative and pheromone-treated cells. Values are from four independent experiments. The graphs in the figure were generated after normalizing the raw Fus3 intensities to the corresponding Spa2-GFP and Spa2^{6xSA}-GFP intensities reported by MaxQuant. The normalized Fus3 intensities were then scaled by dividing by their standard deviations. Experiments in which the cells expressed Spa2-GFP and Spa2^{6xSA}-GFP at the *SPA2* locus (in situ tagged) or from plasmids integrated at the *URA3* locus were scaled independently. Neg stands for negative controls. The p-value shown on the graph is from a two-sample Student's *t*-test computed in R.

partners, we used mass spectrometry (LC-MS/MS) to quantify the amount of proteins that co-immunoprecipitated with Spa2-GFP and Spa2^{6XSA}-GFP in vegetative and pheromone-treated cells. The list of proteins identified in these experiments is available as Supplementary Table 3. The table contains a subset of 288 proteins selected by a Chi-squared test on the spectral counts obtained in 12 independent experiments (including 4 negative controls in which a non-specific antibody was used instead of the anti-GFP antibody). The subset contains known 19 Spa2 interactors such as Bni1, Sla2, and Cdc28, as well as previously unreported candidate interactors such as Fus3, Hog1, and Kar4. Gene ontology analysis of the candidate list shows that genes involved in actin filament regulation and genes involved in RNA localization are enriched (Supplementary Table 3).

To specifically determine whether the six serine to alanine substitutions in Spa2 affects its ability to pull down Fus3 and other candidate interactors, we used the protein intensities, which provide a more sensitive measure of peptide abundance over a greater dynamic range as compared to spectral counts. As shown in Fig. 3, pheromone-treatment greatly increased the pull-down of Fus3 by Spa2-GFP, and to a significantly greater degree, by Spa2^{6XSA}-GFP. The higher apparent affinity of Fus3 for Spa2^{6XSA}-GFP could be the result of a non-productive kinase-substrate interaction, as has been reported for protein kinase C [33], consistent with our conclusion that Fus3 is at least partially responsible for the phosphorylation of Spa2 during the mating response. In addition to Fus3, Pdr5, Mnn11, and Imd2 were identified in this analysis. Unlike Fus3, however, all three of these proteins were pulled down less efficiently by the Spa2^{6XSA}-GFP bait as compared with the Spa2-GFP bait (Student's *t*-test *p*-value < .05). These data are presented in Supplementary Table 3.

3.4. *Spa2^{6XSA}-GFP confers defects in chemotropism and zygote formation*

To determine how chemotropism and zygote formation are affected by the phosphorylation of Spa2 residues S254, S274, S585, S646, S979, and S1263 — the putative targets of Gα/Fus3 regulation — we took time-lapse DIC and fluorescent images of mating mixtures in which *MAT***a** cells expressing either Spa2-GFP or Spa2^{6XSA}-GFP were crossed to wild type *MAT*α cells. We followed *MAT***a** cells that fused with *MAT*α cells after completing cytokinesis and scored them for four behaviors at five-minute intervals: mating projection formation (shmooing), elongation exclusively toward the mating partner, movement of the Spa2 reporter from the cytokinesis site to the chemotropic site, and formation of viable zygotes (Fig. 4). As shown in Fig. 4A–B, 82% of the *MAT***a** Spa2-GFP cells shmooed, and of these, 93% elongated directly toward their partner. In contrast, only 43% of the *MAT***a** Spa2^{6XSA}-GFP cells shmooed ($p < .0001$), and of those that elongated, 40% grew in the wrong direction ($p < .0001$). Zygotes formed by non-shmooing or misoriented *MAT***a** Spa2^{6XSA}-GFP cells appeared to result from fusion at a contact site determined solely by the *MAT*α cells, suggesting a wild type partner can rescue the apparent chemotropic defect conferred by Spa2^{6XSA}.

Although Spa2 is known to be highly concentrated at sites of polarized growth — e.g., the mother-daughter neck of budding cells and the tips of mating projections in cells responding to pheromone — its movement from the cytokinesis site (CKS) to the chemotropic growth site, and ultimately, to the fusion site of mating cells, has never been studied in situ. To standardize our characterization of Spa2 localization in mating cells, we analyzed its movement from the mother-daughter neck (one time point following cytokinesis), to the cell fusion site (one time point before zygote formation) (Fig. 4C). In mating *MAT***a** Spa2-GFP cells, the reporter either appeared to "jump" from the CKS to the fusion site during the 5 min between time points, or, to move along the plasma membrane (PM) directly from the CKS to the fusion site, a phenomenon we call *tracking*. In a small fraction of mating *MAT***a** cells, the path of Spa2-GFP along the PM from the CKS to the fusion site was not direct (i.e, it did not persistently move in one direction), a phenomenon we call *wandering*. In *MAT***a** Spa2^{6XSA}-GFP cells, the movement of the reporter from the CKS to the fusion site was clearly abnormal. As compared to the wild type reporter, Spa2^{6XSA}-GFP jumped much less often (18% vs. 38%; $p < .005$), and wandered much more often (43% vs. 8%; $p < .0001$). Not surprising, it took considerably longer, on average, for Spa2^{6XSA}-GFP to translocate to the fusion site as compared to Spa2-GFP (3.7 ± 0.5 vs. 2.3 ± 0.4 time points; $n \geq 49$; $p = .03$).

The fusion of two mating yeast cells to form a viable zygote is a complex process that requires strict spatiotemporal coordination of signaling elements, structural proteins, and enzymatic activities [3]. During the pre-zygotic stage, mating partners each synthesize new lateral and apical cell wall that is thought to be of distinct composition. This helps prevent the subsequent degradation of the cell wall from occurring outside the zone of contact, and thereby promotes controlled PM fusion. Highly localized delivery of the degradative enzymes is also critical. Any failure in the orchestration of these events can result in cell lysis due to osmotic pressure. In our time-lapse mating mixtures, *MAT***a**

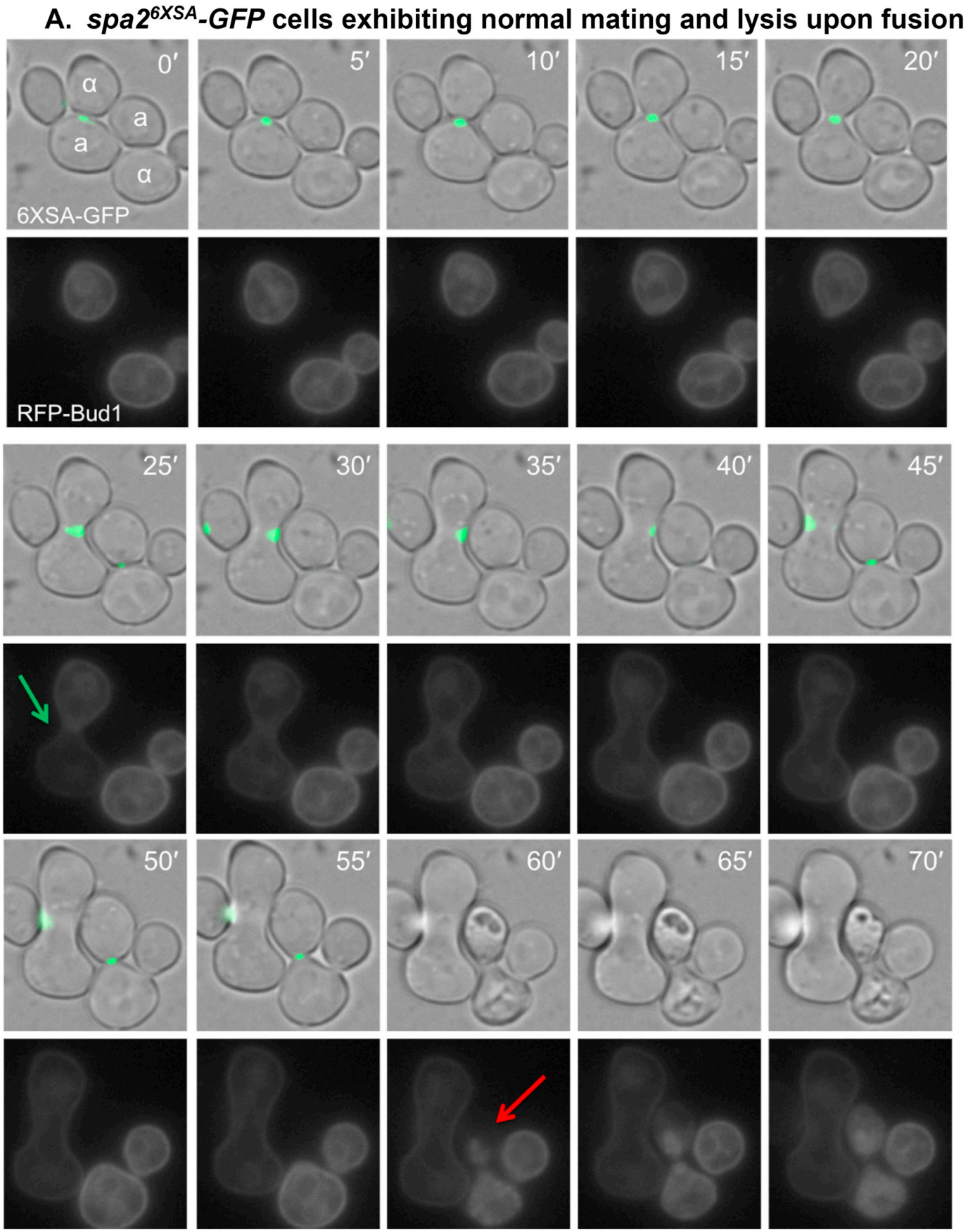

(caption on next page)

Fig. 4. Effect of serine to alanine substitutions at Spa2 positions 254, 274, 585, 646, 979, and 1263 on chemotropism, cell fusion, and Spa2 localization. *MAT***a** *SPA2-GFP* and *MAT***a** *spa2^{6XSA}-GFP* cells were crossed with wild type *MAT*α cells expressing *BUD1-RFP* as a fusion marker, and DIC and fluorescent images were taken at five-minute intervals. **A**. Spa2^{6XSA} confers a defect in cell fusion. Representative images of a *MAT***a** *spa2^{6XSA}-GFP* cell that successfully mated (25′, green arrow) and one that lysed upon fusion (60′, red arrow). **B**. Spa2^{6XSA} confers defects in chemotropic growth. (i) Representative *MAT***a** *SPA2-GFP* cells that exhibit normal chemotropism; (ii) Example of a *MAT***a** *spa2^{6XSA}-GFP* cell that failed to shmoo; (iii) Example of a *MAT***a** *spa2^{6XSA}-GFP* cell that elongated away from its partner. Yellow arrows indicate Spa2^{6XSA}-GFP localization and corresponding growth. **C**. Spa2^{6XSA}-GFP is defective in localization to the chemotropic growth site in mating cells. (i; ii) Examples of Spa2-GFP redistributing from the cytokinesis site to the chemotropic site in mating cells either by jumping (I, red arrows) or tracking (ii, yellow arrows); (iii) Example of Spa2^{6XSA}-GFP wandering behavior. The position of Spa2^{6XSA}-GFP is indicated as polarized at the cell cortex (white arrows) or diffuse within the cytoplasm (white arrowheads) at each time point. White curved arrows indicate the directional change in Spa2^{6XSA}-GFP position between time points. (For interpretation of the references to colour in this figure legend, the reader is referred to the web version of this article.)

Spa2-GFP and *MAT*α cells rarely lysed upon fusion, whereas lysis of both *MAT***a** Spa2^{6XSA}-GFP and *MAT*α partners attempting to fuse was observed relatively often (8% vs. 1.6%; $p < .0001$). This difference was confirmed by quantifying the incidence of fusion-induced lysis in cells removed at hourly intervals from mating mixtures on plates. Zygotes were scored for lysis by their characteristic appearance under phase-contrast microscopy, and for inviability based on their uptake of the vital dye, trypan blue (Supplementary Table 4).

4. Discussion

The pheromone receptor and its G protein are uniformly distributed on the surface and cortex, respectively, of vegetative cells. Pheromone gradients induce polarization of the receptor and G protein to the eventual chemotropic growth site, and this occurs prior to morphogenesis. Once actin-cable-directed secretion begins, nascent receptor and G protein are delivered to the growth site, ultimately concentrating at the tip of the mating projection. We have shown that cells unable to polarize the receptor are defective in gradient sensing [34], and that both polarization of Gα and its interaction with the Kar3 motor protein are required to orient nuclear migration in pheromone-treated cells [35]. Moreover, a number of studies have implicated the Gα-Fus3 interaction in chemotropism: Gα^{DSD} confers defects in gradient sensing [10,17], chemotropic growth [15], pheromone-induced Gβ phosphorylation [10], and Bni1 function in pheromone-treated cells [12]. Together, these results suggest that the receptor and G protein determine the position of the chemotropic growth site in response to the pheromone gradient, whereupon Gα recruits Fus3 to phosphorylate multiple cortical proteins required for chemotropism and cell fusion.

To identify additional Gα-Fus3 targets, we conducted a quantitative phosphoproteomic analysis designed to reveal pheromone-induced phosphorylation sites that are inefficiently phosphorylated in the absence of Gα-Fus3 interaction. We found that a cohort of proteins associated with cell polarity was hypophosphorylated in Gα^{DSD} as compared to control cells 30 min after pheromone treatment. Of the fourteen proteins identified in our screen, eight have known roles in exocytosis (Pea2, Mdr1, and Spa2), endocytosis (Ldb17 and Sla2), polarity (Cdc10), or cell integrity (Ypk1 and Ypk2). Spa2, Pea2, and Sla2 are of particular interest because their putative phospho-sites are MAPK motifs (S/TP), and because they are members, along with Cdc10, of a functional module that regulates polarity (Fig. 1B).

As a first step in testing the biological relevance of the phospho-sites identified in our screen, we created Spa2^{6XSA}, a mutant form of Spa2 that serves as a proxy for the hypophosphorylated Spa2 in Gα^{DSD} cells. A component of the polarisome, Spa2 plays a role in actin cytoskeletal organization during polarized growth in both budding and shmooing cells, and has also been reported to act as a scaffold for the Mkk1 and Mpk1 cell wall integrity kinases in vegetative cells [36]. Deletion of *SPA2* confers an approximately 50% decrease in mating efficiency [37] with a high proportion of mating pairs arresting at the pre-zygote phase [38]. In mating mixtures, *Spa2^{6XSA}* cells exhibited three pronounced phenotypes: defects in gradient sensing, chemotropic growth, and cell fusion. The defect in gradient sensing is evident in the aberrant tracking of the Spa2^{6XSA}-GFP reporter and the high incidence of mutant cells that oriented away from their partners; the fusion defect is evident in the increased frequency of cell lysis. The latter constitutes a catastrophic failure in mating, as it results in the death of both partners. Lysis is the expected outcome if the cell wall remodeling enzymes are not properly localized to the shmoo tip. These results are consistent with the idea that the pheromone-induced phosphorylation of Spa2 is critical to chemotropic growth and cell fusion. It is also possible that the change in the primary sequence of Spa2, and not the absence of phosphorylated sites, confers the observed mating phenotypes. However, it is clear that Spa2^{6XSA}-GFP is at least partially functional, as it localizes to the PM (Fig. 4) and binds to its polarisome partner Bni1 with normal affinity (Supplemental Table 3).

Although we have not yet determined the molecular mechanism underlying the *Spa2^{6XSA}* phenotypes, our data indicate that many proteins, including Spa2, decrease dramatically in pheromone-treated Gα^{DSD} cells. Previously, we reported that Gα^{DSD} has the same effect on the abundance of Gβ [10]. Gα-directed Fus3 phosphorylation may locally inhibit the proteolysis of key chemotropic and polarity factors, and this might indirectly affect the stability of their binding partners. Alternatively, or in addition, dysfunction of polarity proteins in cells induced to polarize their growth might adversely affect a range of proteins in the same functional network.

In conclusion, the observations described here and in published studies support the idea that pheromone-activated Gα recruits active Fus3 to the chemotropic growth site to phosphorylate proteins that serve a variety of mating functions. Local stimulation of actin-cable-directed secretion via the formin protein, Bni1, and the polarisome proteins, Spa2 and Pea2, is expected to strengthen signaling at the shmoo site by positive feedback, as the receptor and G protein are secretory proteins; localized endocytosis contributes to the maintenance of polarity [39]; and cell-integrity signaling likely plays a role in preventing lysis during fusion. We propose that Gα-Fus3 serves as a signaling hub: the MAPK is localized to the incipient shmoo site by receptor/G-protein signaling, where it coordinates multiple processes to effect spatiotemporal regulation of mating. Functional Gα-MAPK interactions have also been demonstrated in *Dictyostelium discoideum* [40,41], suggesting that similar mechanisms exist in multicellular organisms.

Supplementary data to this article can be found online at https://doi.org/10.1016/j.jprot.2019.103467.

B.

i. *SPA2-GFP* cell exhibiting normal chemotropism

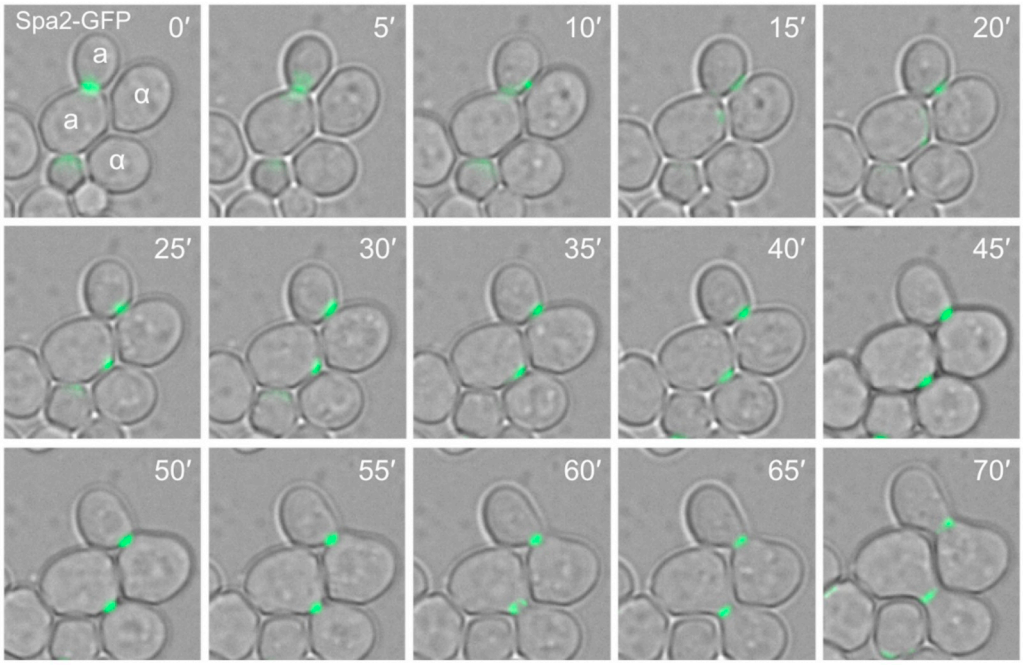

Shmoo Formation		
	WT	6XSA
Normal	41	21
None	9	28
n	50	49
p Value		0.0001

ii. *spa2^{6XSA}-GFP* cell failing to shmoo

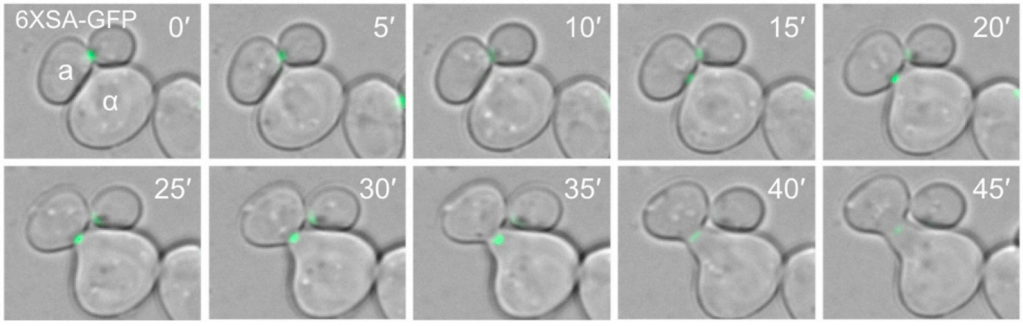

iii. *spa2^{6XSA}-GFP* cell elongating away from its partner

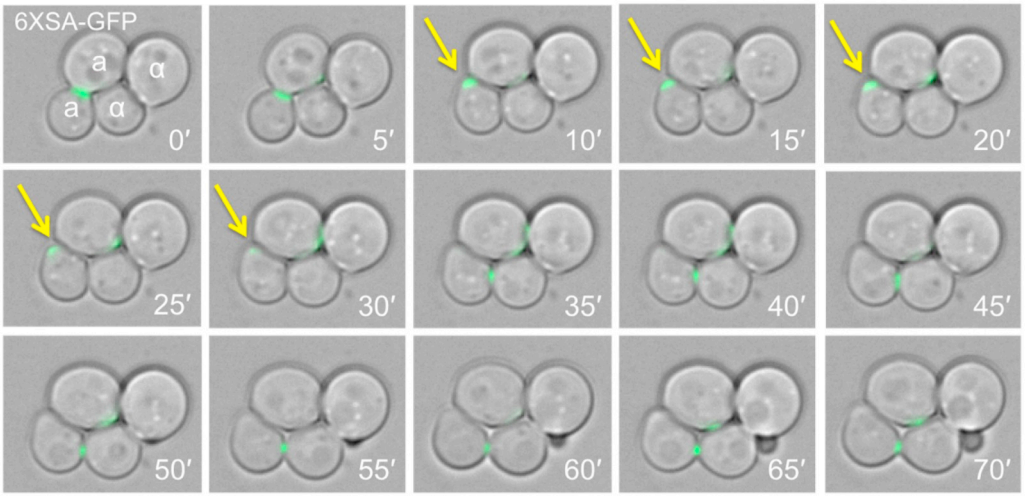

Elongation Direction Relative to Partner		
	WT	6XSA
Toward	40	18
Away	3	12
n	43	30
p Value		0.0001

Fig. 4. (*continued*)

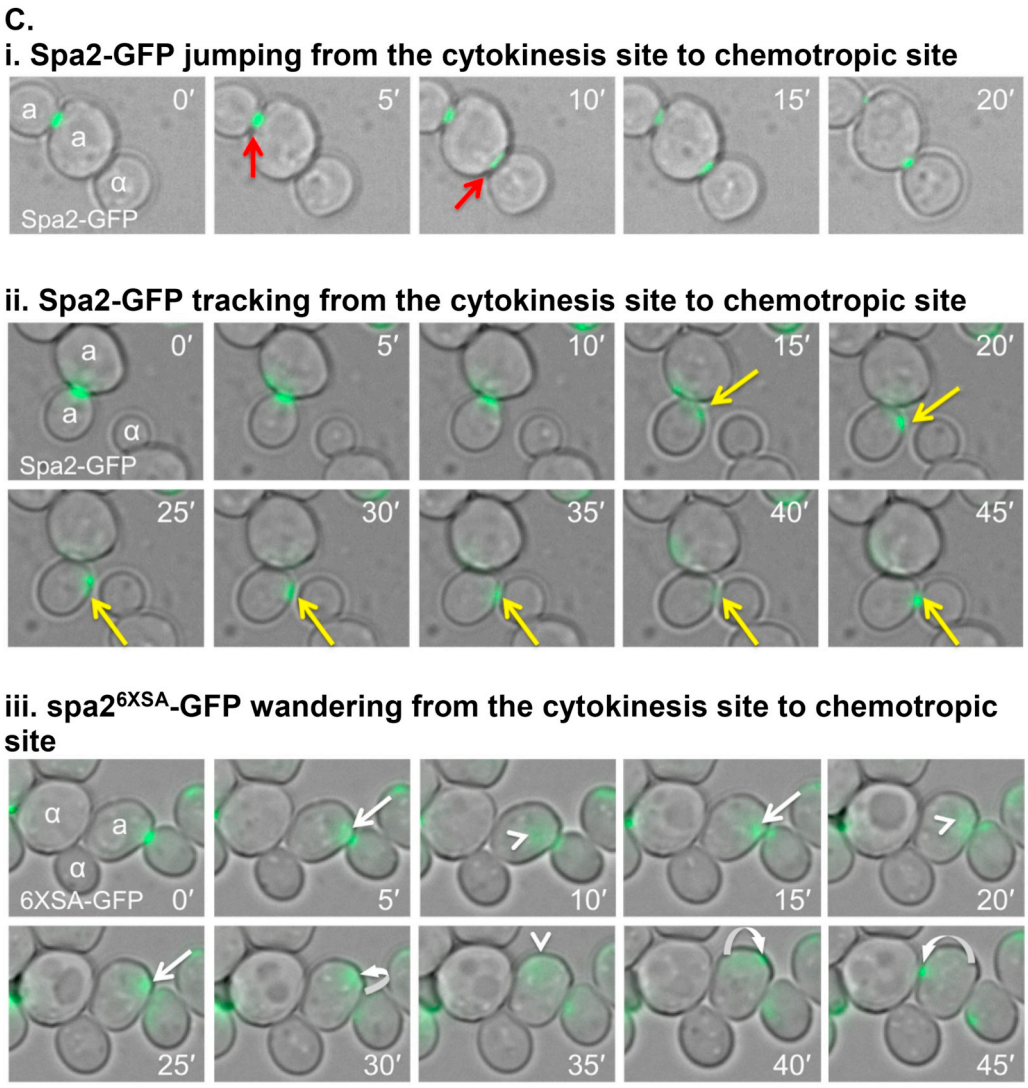

Spa2-GFP Movement to Fusion Site

	WT	6XSA
Jump	19	9
Incremental	31	40
n	50	49
p Value		0.0046

Nature of Spa2-GFP Incremental Movement to Fusion Site

	WT	6XSA
Track	27	23
Wander	4	17
n	31	40
p Value		0.0001

Fig. 4. (*continued*)

Acknowledgements

This work was supported by National Science Foundation (NSF) grants 1415589 and 1818067 (to DES), and funding from University of Essex, United Kingdom to establish a proteomics laboratory (to MVM).

Author contributions

NW and MM: strain construction for the SILAC labeling and all proteomic procedures and analysis.

AI and NC: *SPA2* mutagenesis and strain construction.

RDF: Strain construction and analysis of *Spa2*^{6XSA}-GFP phenotypes; Spa2^{6XSA}-GFP pull-downs.

DS and MM: Project direction and manuscript.

Declaration of Competing Interests

The authors declare no competing interests.

References

[1] L. Bardwell, A walk-through of the yeast mating pheromone response pathway, Peptides 25 (2004) 1465–1476.
[2] E.A. Elion, Pheromone response, mating and cell biology, Curr. Opin. Microbiol. 3 (2000) 573–581.
[3] A.M. Tartakoff, Cell biology of yeast zygotes, from genesis to budding, Biochim. Biophys. Acta 1853 (2015) 1702–1714.
[4] A.C. Butty, P.M. Pryciak, L.S. Huang, I. Herskowitz, M. Peter, The role of Far1p in linking the heterotrimeric G protein to polarity establishment proteins during yeast mating, Science 282 (1998) 1511–1516.
[5] A. Nern, R.A. Arkowitz, A Cdc24p-Far1p-Gbetagamma protein complex required for yeast orientation during mating, J. Cell Biol. 144 (1999) 1187–1202.
[6] D. Pruyne, A. Bretscher, Polarization of cell growth in yeast. I. Establishment and maintenance of polarity states, J. Cell Sci. 113 (Pt 3) (2000) 365–375.
[7] D. Pruyne, A. Bretscher, Polarization of cell growth in yeast, J. Cell Sci. 113 (Pt 4) (2000) 571–585.
[8] H.O. Park, E. Bi, Central roles of small GTPases in the development of cell polarity in yeast and beyond, Microbiol. and Mol. Biol. Revi.: MMBR 71 (2007) 48–96.
[9] R. Dorer, P.M. Pryciak, L.H. Hartwell, Saccharomyces cerevisiae cells execute a default pathway to select a mate in the absence of pheromone gradients, J. Cell Biol. 131 (1995) 845–861.
[10] M.V. Metodiev, D. Matheos, M.D. Rose, D.E. Stone, Regulation of MAPK function by direct interaction with the mating-specific Galpha in yeast, Science 296 (2002) 1483–1486.
[11] E. Blackwell, I.M. Halatek, H.J. Kim, A.T. Ellicott, et al., Effect of the pheromone-responsive G(alpha) and phosphatase proteins of Saccharomyces cerevisiae on the subcellular localization of the Fus3 mitogen-activated protein kinase, Mol. Cell. Biol. 23 (2003) 1135–1150.
[12] D. Matheos, M. Metodiev, E. Muller, D. Stone, M.D. Rose, Pheromone-induced polarization is dependent on the Fus3p MAPK acting through the formin Bni1p, J. Cell Biol. 165 (2004) 99–109.
[13] D.E. Stone, G.M. Cole, M. de Barros Lopes, M. Goebl, S.I. Reed, N-myristoylation is required for function of the pheromone-responsive G alpha protein of yeast: conditional activation of the pheromone response by a temperature-sensitive N-myristoyl transferase, Genes Dev. 5 (1991) 1969–1981.
[14] J. Song, H.G. Dohlman, Partial constitutive activation of pheromone responses by a palmitoylation-site mutant of a G protein alpha subunit in yeast, Biochemistry 35

(1996) 14806–14817.
[15] R. DeFlorio, M.E. Brett, N. Waszczak, E. Apollinari, et al., Phosphorylation of Gbeta is crucial for efficient chemotropism in yeast, J. Cell Sci. 126 (2013) 2997–3009.
[16] E. Li, M.J. Cismowski, D.E. Stone, Phosphorylation of the pheromone-responsive Gbeta protein of Saccharomyces cerevisiae does not affect its mating-specific signaling function, Mol. Gen. Genet. 258 (1998) 608–618.
[17] B. Errede, L. Vered, E. Ford, M.I. Pena, T.C. Elston, Pheromone-induced morphogenesis and gradient tracking are dependent on the MAPK Fus3 binding to Galpha, Mol. Biol. Cell 26 (2015) 3343–3358.
[18] G.R. Sherman, J. Fink, B. Hicks, Cold Spring Harbor Laboratory, Cold Spring Harbor Laboratory, 1986.
[19] R.D. Gietz, R.H. Schiestl, High-efficiency yeast transformation using the LiAc/SS carrier DNA/PEG method, Nat. Protoc. 2 (2007) 31–34.
[20] H. Ito, Y. Fukuda, K. Murata, A. Kimura, Transformation of intact yeast cells treated with alkali cations, J. Bacteriol. 153 (1983) 163–168.
[21] Frederick M. Ausubel, Roger Brent, Robert E. Kingston, David D. Moore, J.G. Seidman, Kevin Struhl, Current Protocols in Molecular Biology, John Wiley and Sons Inc, New York, 1994.
[22] G.M. Cole, D.E. Stone, S.I. Reed, Stoichiometry of G protein subunits affects the Saccharomyces cerevisiae mating pheromone signal transduction pathway, Mol. Cell. Biol. 10 (1990) 510–517.
[23] S.I. Reed, J.A. Hadwiger, A.T. Lörincz, Protein kinase activity associated with the product of the yeast cell division cycle gene CDC28, Proc. Natl. Acad. Sci. U. S. A. 82 (1985) 4055–4059.
[24] R.A. Arkowitz, N. Lowe, A small conserved domain in the yeast Spa2p is necessary and sufficient for its polarized localization, J. Cell Biol. 138 (1997) 17–36.
[25] J. Cox, M. Mann, MaxQuant enables high peptide identification rates, individualized p.p.b.-range mass accuracies and proteome-wide protein quantification, Nat. Biotechnol. 26 (2008) 1367–1372.
[26] J. Cox, N. Neuhauser, A. Michalski, R.A. Scheltema, et al., Andromeda: a peptide search engine integrated into the MaxQuant environment, J. Proteome Res. 10 (2011) 1794–1805.
[27] G. Metodieva, N.C. Nogueira-de-Souza, C. Greenwood, K. Al-Janabi, et al., CD74-dependent deregulation of the tumor suppressor scribble in human epithelial and breast cancer cells, Neoplasia 15 (2013) 660–668.
[28] L. Alldridge, G. Metodieva, C. Greenwood, K. Al-Janabi, et al., Proteome profiling of breast tumors by gel electrophoresis and nanoscale electrospray ionization mass spectrometry, J. Proteome Res. 7 (2008) 1458–1469.
[29] S.E. Ong, B. Blagoev, I. Kratchmarova, D.B. Kristensen, et al., Stable isotope labeling by amino acids in cell culture, SILAC, as a simple and accurate approach to expression proteomics, Mol. Cell. Proteomics 1 (2002) 376–386.
[30] R. Balakrishnan, J. Park, K. Karra, B.C. Hitz, et al., YeastMine–an integrated data warehouse for Saccharomyces cerevisiae data as a multipurpose tool-kit, Database (Oxford) 2012 (2012) bar062.
[31] K. Tedford, S. Kim, D. Sa, K. Stevens, M. Tyers, Regulation of the mating pheromone and invasive growth responses in yeast by two MAP kinase substrates, Current Biol.: CB 7 (1997) 228–238.
[32] X. Li, S.A. Gerber, A.D. Rudner, S.A. Beausoleil, et al., Large-scale phosphorylation analysis of alpha-factor-arrested Saccharomyces cerevisiae, J. Proteome Res. 6 (2007) 1190–1197.
[33] R.F. Sommese, S. Sivaramakrishnan, Substrate affinity differentially influences protein kinase C regulation and inhibitor potency, J. Biol. Chem. 291 (2016) 21963–21970.
[34] A. Ismael, W. Tian, N. Waszczak, X. Wang, et al., Gβ promotes pheromone receptor polarization and yeast chemotropism by inhibiting receptor phosphorylation, Sci. Signal. 9 (2016) ra38.
[35] S.V. Zaichick, M.V. Metodiev, S.A. Nelson, O. Durbrovskyi, et al., The mating-specific Galpha interacts with a kinesin-14 and regulates pheromone-induced nuclear migration in budding yeast, Mol. Biol. Cell 20 (2009) 2820–2830.
[36] F. van Drogen, M. Peter, Spa2p functions as a scaffold-like protein to recruit the Mpk1p MAP kinase module to sites of polarized growth, Curr. Biol. 12 (2002) 1698–1703.
[37] R. Dorer, C. Boone, T. Kimbrough, J. Kim, L.H. Hartwell, Genetic analysis of default mating behavior in Saccharomyces cerevisiae, Genetics 146 (1997) 39–55.
[38] A.E. Gammie, V. Brizzio, M.D. Rose, Distinct morphological phenotypes of cell fusion mutants, Mol. Biol. Cell 9 (1998) 1395–1410.
[39] J. Valdez-Taubas, H.R. Pelham, Slow diffusion of proteins in the yeast plasma membrane allows polarity to be maintained by endocytic cycling, Curr. Biol. 13 (2003) 1636–1640.
[40] B. Raisley, H.N. Nguyen, J.A. Hadwiger, G{alpha}5 subunit-mediated signalling requires a D-motif and the MAPK ERK1 in Dictyostelium, Microbiology 156 (2010) 789–797.
[41] H.N. Nguyen, J.A. Hadwiger, The Galpha4 G protein subunit interacts with the MAP kinase ERK2 using a D-motif that regulates developmental morphogenesis in Dictyostelium, Dev. Biol. 335 (2009) 385–395.
[42] D. Szklarczyk, A.L. Gable, D. Lyon, A. Junge, et al., STRING v11: protein-protein association networks with increased coverage, supporting functional discovery in genome-wide experimental datasets, Nucleic Acids Res. 47 (2019) D607–D613.